Title: Interferon stimulated genes mark pathogenic cells of the myelopoietic response to sterile tissue injury in mice and humans.

Authors: David M. Calcagno[1*], Richard P. Ng Jr.[2*], Avinash Toomu[2], Kenneth Huang[2], Aaron D. Aguirre[3], Lori B. Daniels[2], Zhenxing Fu[2], Kevin R. King[1,2]

Affiliations :

[1]Department of Bioengineering, Jacobs School of Engineering, University of California San Diego, La Jolla, CA, USA.

[2]Division of Cardiology and Cardiovascular Institute, Department of Medicine, University of California San Diego, La Jolla, CA, USA.

[3]Cardiology Division, Massachusetts General Hospital, Harvard Medical School, Boston, Massachusetts, USA.

* Authors contributed equally.

Corresponding author: Kevin R. King, MD, PhD
University of California San Diego
9500 Gilman Dr. MC 0412
La Jolla, CA 92093
Tel: 617-869-9339
krking@ucsd.edu

ABSTRACT

Sterile tissue injury recruits myeloid cells (neutrophils and monocytes) from the bone marrow by stimulating a process known as emergency myelopoiesis. It is commonly assumed that myeloid cells activate proinflammatory signaling pathways within the injured tissue after sensing innate immune-activating molecules in the local microenvironment. Here, we show that pathogenic innate immune signaling in myeloid cells begins far from the site of injury, at their origins in the bone marrow. Using myocardial infarction (MI) as a model of sterile injury, we profiled single cell transcriptomes of >50,000 myeloid cells and found evidence of type I interferon signaling characterized by expression of interferon stimulated genes (ISGs) in a subset of neutrophils and monocytes in the heart, blood, and bone marrow after MI. We validated the findings in humans by quantifying ISG-expression in myeloid cells of patients presenting with acute MI, which revealed ISG levels far exceed that of healthy subjects and are comparable to patients with the interferon-associated autoimmune disease, systemic lupus erythematous. The identification of remote innate immune education raises important questions about how distant tissue injury activates interferon signaling in the hematopoietic compartment. Clinically, our data provide a strategy for quantifying pathogenic subsets of emergency myelopoietic cells in the blood as a biomarker that may identify patients who have disproportionately worse outcomes or who may benefit from immune modulatory therapy after acute MI.

Myelopoiesis is the process by which hematopoietic stem and progenitor cells in the bone marrow proliferate, differentiate, and mature into neutrophils and monocytes that patrol the vasculature and distant organs at steady state[1-3]. Heterogeneity in peripheral blood leukocytes is thought to arise primarily via differences in maturation (e.g. based on immunophenotyping of Ly6C)[4,5]. Sterile tissue injury provokes the bone marrow to supply increased numbers of neutrophils and monocytes through a process known as emergency myelopoiesis (EM)[6-9]. When myeloid cells reach the site of injury and infiltrate damaged tissue, they are thought to be educated by interactions with local microenvironmental factors such as damage associated molecular patterns that induce innate immune signaling pathways leading to production of proinflammatory cytokines and chemokines[10-13]. Here, we show that innate immune activation begins in the bone marrow, far from the site of injury, at the origins of emergency hematopoiesis, leading to previously unrecognized heterogeneity in the blood that can be quantified in mouse and humans.

Using myocardial infarction (MI) as a model of sterile injury, we performed single cell RNA-Seq on 55,687 neutrophils, monocytes, and macrophages from the heart, blood, and bone marrow of WT mice on days 1-4 after MI as well as from human blood of patients presenting with acute MI. Previously, we discovered that MI induces a deleterious type I interferon response in monocyte-derived macrophages of the infarcted heart on day 4 after MI, and genetic or pharmacologic inhibition of type I interferon signaling was protective by reducing ventricular dilation and improving survival[14]. Here we show that neutrophils and monocytes from the bone marrow, blood and heart exist as mirrored

populations of cells expressing (ISG+) or not expressing (ISG-) interferon stimulating genes after MI. In human patients presenting with acute MI, we find analogous ISG+ and ISG- myeloid cells at levels far beyond healthy subjects and comparable to patients with systemic lupus erythematous, a prototypical interferon-associated autoimmune disease. To enable translational studies, we defined an ISG product (ISGP) biomarker that accounts for cell number and ISG expression and can be quantified in patients to determine whether individuals with high ISGP have preferentially worse clinical outcomes and may benefit from immune modulatory therapy. Together, our results show that remote sterile tissue injury induces pathogenic ISG-expressing myeloid subsets of the EM response in mice and humans.

RESULTS

Single cell transcriptomic analysis of myeloid cells from the heart, blood, and bone marrow after myocardial infarction in mice and humans. To model the sterile injury of MI in mice, we performed permanent ligation of the left anterior coronary artery, harvested the infarcted cardiac tissue, blood, and bone marrow on days 1-4 after MI, sorted live single non-erythrocytes ($Dapi^{LOW}$, $Ter119^{LOW}$), and performed microfluidic droplet-based single cell RNA-Seq using inDrop or 10X Genomics barcoding platforms **(Fig. 1a, Table 1)**. Coarse clustering and bioinformatic subsetting revealed a neutrophil-predominant distribution on day 1 **(Fig. 1b)** and a monocyte-macrophage-predominant distribution on day 4 within the infarcted heart **(Fig. 1c)** consistent with previously reported data based on flow cytometry[15]. We bioinformatically isolated neutrophils and monocytes and separately reclustered them to investigate their subsets. Using this method, we

analyzed 59,646 single cells from the mouse bone marrow, blood, and heart **(Fig. 1d),** and human blood leukocytes collected in the setting of acute MI **(Fig. 1e).**

Neutrophil heterogeneity within the infarcted heart. Neutrophils are short-lived, first responders to sterile tissue injuries including MI. In contrast to monocytes and macrophages, little is known about how neutrophils diversify and specialize after entering the injured heart[16,17]. We bioinformatically subset neutrophils (*S100a8, S100a9, Retnlg, Mmp9*, *Cxcr2*)^{HI}, renormalized, scaled, and reclustered them to explore neutrophil heterogeneity and discovered five distinct intracardiac neutrophil subsets with distinct temporal patterns **(Fig. 2a-g, Extended Data Fig. 1a-c, Table 2)**. The parent neutrophil subset (Hrt-N1*),* characterized by expression of *Retnlg*, was present in every sample at every time point and mirrored blood neutrophils **(Fig. 2a-c, Extended Data Fig. 1c, Table 3a)**. Hrt-N2 neutrophils expressed interferon-stimulated genes (ISGs), which was surprising because previous work showed ISG expression predominantly in monocyte-derived macrophages on day 4 after MI[14]. Nevertheless, subsetting and reclustering revealed that ISG-expressing neutrophils are identifiable as early as day 1 **(Fig. 2a,b,d, Extended Data Fig. 1c, Table 3b)**, demonstrating that type I interferon signaling is active in multiple myeloid lineages after MI. The Hrt-N3 subset expressed genes associated with NFκB activation, including *Nfkb1, Icam1, Il1a, Sod2, and Tnip1* **(Fig. 2a,b,e, Extended Data Fig. 1c, Table 3c)** while the Hrt-N4 population expressed genes associated with *Hif-1α* activation*,* including *Egln3, Hilpda, and Vegfa* **(Fig. 2a,b,f, Extended Data Fig. 1c, Table 3d)***[18]*. Both Hrt-N3 and Hrt-N4 were prominent on day 1 but declined by day 4 in concert with emergence of a new neutrophil subset (Hrt-N5), characterized by

expression of *Siglecf* **(Fig. 2a,b,g, Extended Data Fig. 1c, Table 3e)**. Although *Siglecf* is best known as an eosinophil marker and is often gated against when sorting neutrophils, recent single cell RNA-Seq work identified a similar SiglecF-expressing neutrophil in the context of murine lung cancer[19]. Indeed, we were able to confirm, using surface antibody staining, that neutrophils (Cd11b+, Ly6G+) are separable into Siglecf^{HI} and Siglecf^{LOW} subpopulations and can be FACS sorted for qPCR validation of the single cell RNA-Seq findings **(Extended Data Fig. 2)**.

Since previous work found the interferon response to be detrimental after MI[14], we bioinformatically isolated ISG+ and ISG- neutrophils and reclustered them to enable comparisons. Surprisingly, we independently recovered all of the same neutrophil subsets in ISG+ as ISG- **(Fig. 2h-i)** populations, suggesting that ISG-expression does not restrict the intracardiac specialization potential of neutrophils. To investigate transitions between neutrophil subsets, we performed pseudotime trajectory analysis (Monocle 3.0) on a down-sampled population of cells (n = 5,000 cells) from post-MI day 4 data[20]. Whether analyzed together or individually, ISG+ and ISG- neutrophils resulted in mirrored trajectories **(Fig. 2l, Extended Data Fig. 2a-d),** reinforcing the view that ISG-expression is orthogonal to the other neutrophil phenotypes observed. To examine how ISG expression varies along the neutrophil maturation axis, we compared expression to *Retnlg* and *Siglecf* **(Fig. 2m, Extended Data Fig. 3)** and found that recently-infiltrated *Retnlg*^{HI}*Siglecf*^{LOW} neutrophils expressed the highest levels of ISGs. Taken together, these findings demonstrated that MI induces a subset of neutrophils to become interferon-inducible cells (nIFNICs), that ISG expression does not limit intracardiac differentiation potential, and that nIFNICs may express ISGs prior to entry into the infarcted heart.

Monocyte-macrophage heterogeneity within the infarcted heart. We next bioinformatically isolated monocytes and macrophages and reclustered them revealing monocytes (expressing *Ccr2, Plac8,* and *Ms4a4c)* and intracardiac macrophage subsets **(Fig. 3a-d)**. Monocytes spontaneously clustered into ISG+ (Hrt-m1) and ISG- populations (Hrt-m2). We termed the ISG+ cells monocyte-derived interferon-inducible cells (mIFNICs) to distinguish them from neutrophil nIFNICs. Infarct macrophages divided into Hrt-M1 "proinflammatory" (expressing *C1qa C1qb, Mrc1,* and *Ctsd*), Hrt-M2 "reparative" (expressing *Arg1* and *Vegfa*), Hrt-M3 NSG+ (expressing the Nrf2-stimulated genes (NSGs), *Gclm* and *Slc40a1*), and Hrt-M4 proliferative populations **(Table 4a-e).** Superimposed on these macrophage subsets were ISG-expressing macrophages as well as previously recognized orthogonal gene expression programs including antigen presenting MHCII-related genes and NFκB-regulated proinflammatory cytokines We did not find recently reported "resident cardiac macrophage" marker genes, most likely because we analyzed early time points before resident macrophages have infiltrated the infarct from the surviving myocardium **(Extended Data Fig. 4)**.

Because interferon signaling was shown to play a pathologic role after MI, we bioinformatically isolated ISG+ and ISG- cells and reclustered them **(Fig. 3e-g)**. Similar to intracardiac neutrophils, this revealed mirrored ISG+ and ISG- populations, each containing all of the underlying monocyte-macrophage subsets except the ISG-expressing Hrt1-m2 (as expected), and NSG-expressing Hrt-M3 (examined mechanistically in an accompanying manuscript), which were restricted to ISG-

macrophages. Analogous to neutrophils, pseudotime analysis of post-MI day 4 samples showed expression of ISGs was highest in recently-infiltrated cells (monocytes) expressing *Plac8* and *Ms4a4c*, and declined in mature macrophages expressing *Pf4* and *Spp1* **(Fig. 3h, Extended Data Fig. 5)**. Taken together, this demonstrates that ISG+ and ISG- cells have the same differentiation potential with the exception that only ISG- express NSGs; and that mIFNICs, like nIFNICs, may express ISGs prior to entry into the infarcted heart.

ISG expression by neutrophil and monocyte subsets in the peripheral blood after MI

Since ISGs were expressed by recently-entered intracardiac leukocytes from two myeloid lineages, we considered the possibility that ISGs are expressed in the blood prior to reaching the infarcted heart. Indeed, when we performed single cell RNA-Seq of blood leukocytes on days 1-4 after MI, we identified ISG+ and ISG- subsets of neutrophils **(Fig. 4a,c)** and monocytes **(Fig. 4b,d)** in the circulation[4,5]. In the case of monocytes, we observed ISG+ cells across the continuum of maturation, from immature Ly6C^{HI}Nr4a1^{LOW} to mature Ly6C^{LOW}Nr4a1^{HI}, which depends on expression of C/EBPβ and Nr4a1[4,5]. Together, these results suggested that ISGs may be activated prior to entering the peripheral blood.

ISG expression neutrophil and monocyte subsets in the bone marrow after MI

Since ISG expression was identified in subsets of neutrophils and monocytes in the heart and blood after MI, we tested the hypothesis that they become activated within the bone marrow, where they originate from a common myeloid progenitor during the emergency myelopoietic response. We performed single cell RNA-Seq on hematopoietic cells on days 1-3 after MI and found ISG expression in subsets of developing neutrophils and monocytes. Cluster analysis identified ISG- immature neutrophils (BM-N1) expressing *Camp* and *Chil3,* a spontaneously clustering ISG+ population (BM-N2), and mature neutrophils (BM-N3) expressing *Ccl6* and *Clec4d* **(Fig. 5a-b, Extended Data Fig. 6)**. We bioinformatically isolated ISG+ and ISG- cells, separately reclustered them, and recovered ISG+ neutrophils spanning the spectrum of immature and mature neutrophils **(Fig. 5c)**. Pseudotime analysis confirmed this finding by defining a monotonic progression from immature BM-N1 to mature BM-N3 neutrophils **(Fig. 5d)** and demonstrating that ISG expression increased as BM-N1 neutrophils mature **(Fig. 5e)**. We independently analyzed published single cell transcriptomes of naïve mouse bone marrow neutrophils but did not identify ISG-expressing neutrophil clusters **(Extended Data Fig. 7)**. Finally, we arranged and plotted neutrophil transcriptomes from all three compartments, which revealed MI-induced ISG-expressing subsets gradually increase in ISG expression magnitude from bone marrow to blood to heart **(Fig 5f)**.

We performed a similar analysis on bone marrow monocytes. After subsetting and reclustering, we observed immature monocytes (BM-m1) expressing *Ly6c2* and *Lgals1*, ISG-expressing monocytes (BM-m2), and mature monocytes (BM-m3) expressing *Cx3cr1* and *Apoe* **(Fig. 5g-h)**. The ISG+ monocytes could be subset and reclustered to recover the underlying ISG+ immature and ISG+ mature monocytes **(Fig. 5i)**, which again

demonstrated that activation of the interferon transcriptional program is orthogonal to maturation and does not limit or bias cellular differentiation potential. Pseudotime analysis confirmed the monotonic progression from immature BM-m1 to mature BM-m3 monocytes **(Fig. 5j)**, the later of which closely matched circulating cells in the blood. As anticipated, ISG expression increased as bone marrow monocytes mature **(Fig. 5k)**. Similar to neutrophils, we arranged and plotted monocyte transcriptomes from all three compartments, which revealed that MI-induced ISG-expressing subsets gradually increase in ISG expression magnitude from bone marrow to blood to heart **(Fig 5l)**. We were unable to detect ISG expression in progenitors with any statistical confidence, most likely because they differentiate into neutrophils and monocytes before ISGs increase to levels detectable by single cell RNA-Seq. Nevertheless, the most parsimonious explanation for our data is that ISG expression begins before or at the granulocyte-macrophage progenitors (GMPs) **(Extended Data Fig. 7)**.

ISG+ neutrophils and monocytes are detectable in human blood after MI

When MI was first shown to induce a type I interferon response, attention was focused exclusively on the heart, a clinically-inaccessible tissue that did not permit translational studies to test its relevance in humans. Our new data now show that ISG+ cells can be measured in the peripheral blood, which allowed us to test whether human neutrophils and monocytes express ISGs after MI. We collected peripheral blood leukocytes from a patient 48 hours after presenting with chest pain and elevated blood cardiac troponin levels signifying a non-ST elevation MI (NSTEMI). Single cell RNA-Seq was performed

and neutrophils and monocytes were bioinformatically subset as described above for mouse samples. We found 29% ISG+ neutrophils **(Fig. 6a)** and 20% ISG+ monocytes **(Fig. 6b)** in post-MI human blood samples. We also independently analyzed 40,246 published healthy human single cell RNA-Seq transcriptomes and observed an average of 3% ISG+ cells **(Fig. 6c, Extended Data Fig. 8)** with several samples exhibiting no coordinated ISG expression. Finally, we independently analyzed published single cell transcriptomic data from 8 patients with the interferon-associated autoimmune disease SLE and detected 18% ISG+ monocytes **(Fig. 6d)**, which was significantly more than healthy individuals, yet still less than what we observed after MI. To account for the number of ISG+ cells and extent of ISG expression per cell, we defined an ISG product (ISGP) as defined in the detailed methods. Analysis of ISG scores and ISGP for each sample revealed that MI and lupus patients each have significantly greater ISGPs compared to healthy donors **(Fig. 6e,f)**.

DISCUSSION

Our data demonstrate that ischemia in the heart induces type I interferon signaling in the bone marrow, far from the site of tissue injury. We show this has translational significance because ISG+ cell subsets can be measured in the peripheral blood of patients presenting with acute MI. Single cell transcriptomics was essential for discrimination of ISG+ and ISG- emergency myeloid cell populations because sensitive and specific antibodies for flow cytometric analysis of this pathway are lacking and because ensemble measurement techniques obscure myeloid cell subsets[21,22]. Our data demonstrate that emergency

myeloid cells exhibit unrecognized functional heterogeneity with pathologic significance because ISGs include proinflammatory cytokines and chemokines[22,23] and because genetic or pharmacologic inhibition of interferon signaling was previously shown to reduce post-MI inflammation and protect against adverse ventricular remodeling and death due to ventricular rupture[14].

Our results raise several mechanistic questions for future studies. How does MI initiate interferon signaling in the distant bone marrow and why does it affect only a subset of maturing myeloid cells? Previous studies showed soluble stimuli such as exogenous poly(I:C)[23,24] or endogenous IL1β[25] can induce proliferation of bone marrow stem and progenitor cells, but it remains unclear how a systemic and diffusible substance would activate some but not all neutrophils and monocytes. Sympathetic discharge and adrenergic signaling would provide a more spatiotemporally localized mechanism, but it is not known to induce type I interferon signaling or initiate ISG expression[26]. We and others observed that ISG expression in the heart was dramatically decreased in cGas$^{-/-}$ and Sting$^{gt/gt}$ mice after MI suggesting that double stranded DNA may be an important stimulus[14,27]. Irf3-activating signals downstream of cGAS-dependent DNA sensing are gap junction permeable and may mediate contact-dependent intercellular communication[28,29], and this may involve bone marrow niche cells[30,31]. Alternatively, cell-autonomous Irf3 activation resulting from DNA damage[32], micronuclei[33,34], or transient nuclear rupture[35,36] could provide a spatially localized activation mechanism.

From a clinical perspective, our data provide the first direct evidence that type I interferon signaling is activated by MI in humans. The ability to quantify ISG expression in peripheral blood leukocyte subsets will enable future studies to explore its relationship to clinical

outcomes and response to therapies. Using ISGP, one can now test whether patients with an excessive type I interferon response to MI go on to have worse outcomes from arrhythmias, heart failure, or recurrent MI. It is also possible to compare steady state ISGP to established inflammatory biomarkers associated with cardiovascular risk such as high sensitivity C reactive protein (hs-CRP)[37,38]. Recent studies have demonstrated that anti-cytokine therapy targeting IL1β can reduce recurrent cardiovascular events and it has been suggested that subsets of patients in whom excessive inflammation is a driver of pathology may preferentially benefit[39]. Whether quantification of ISGP can stratify patient populations to identify those who may preferentially benefit from anti-cytokine or immune modulatory therapy can now be tested. Finally, if ISGP predicts worse outcomes, the causative role of type I interferons can be tested using anti-IFNAR therapy, which exhibited acceptable safety profiles during chronic administration in phase 3 clinical trials for lupus[40].

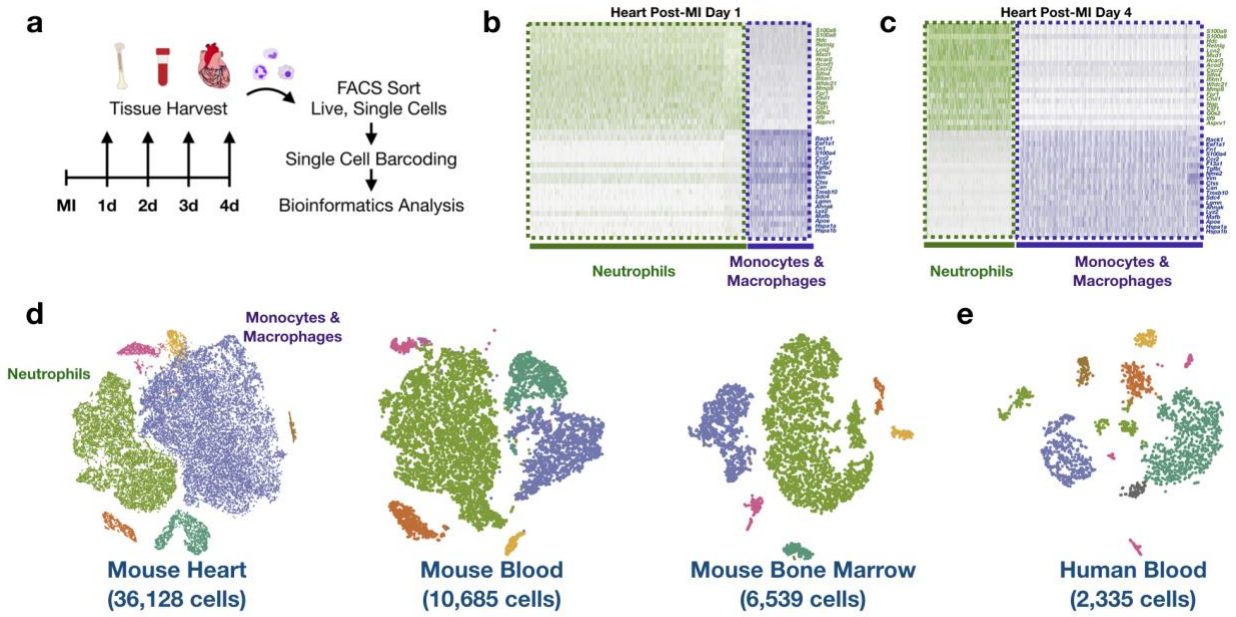

Figure 1. Experimental design. a) Mice were subjected to MI by permanent coronary ligation and bone marrow, blood, and heart tissue was harvested on post-MI days 1, 2 and 4 (n = 55,687 cells). FACS sorting isolated single live non-RBCs for single cell RNA-Seq followed by bioinformatic subsetting of myeloid cells. **b-c)** Representative heatmaps of infarct neutrophils (green) and monocytes/macrophages (purple) on **b)** neutrophil-predominant day 1 and **c)** monocyte-predominant day 4 after MI. Heatmaps show z-score ranging from -2.5 (white), 0 (grey), and +2.5 (green: neutrophils, blue: monocytes and macrophages). **d)** t-SNE maps of mouse tissue compartments across days - mouse heart (36,128 single cells), blood (10,685 single cells), and bone marrow (10,685 single cells). **e)** t-SNE map of human blood (2,335 single cells). Data shown are mean +/- s.e.m. ** *P < .01,* ****P<0.0001, unpaired student t-test.

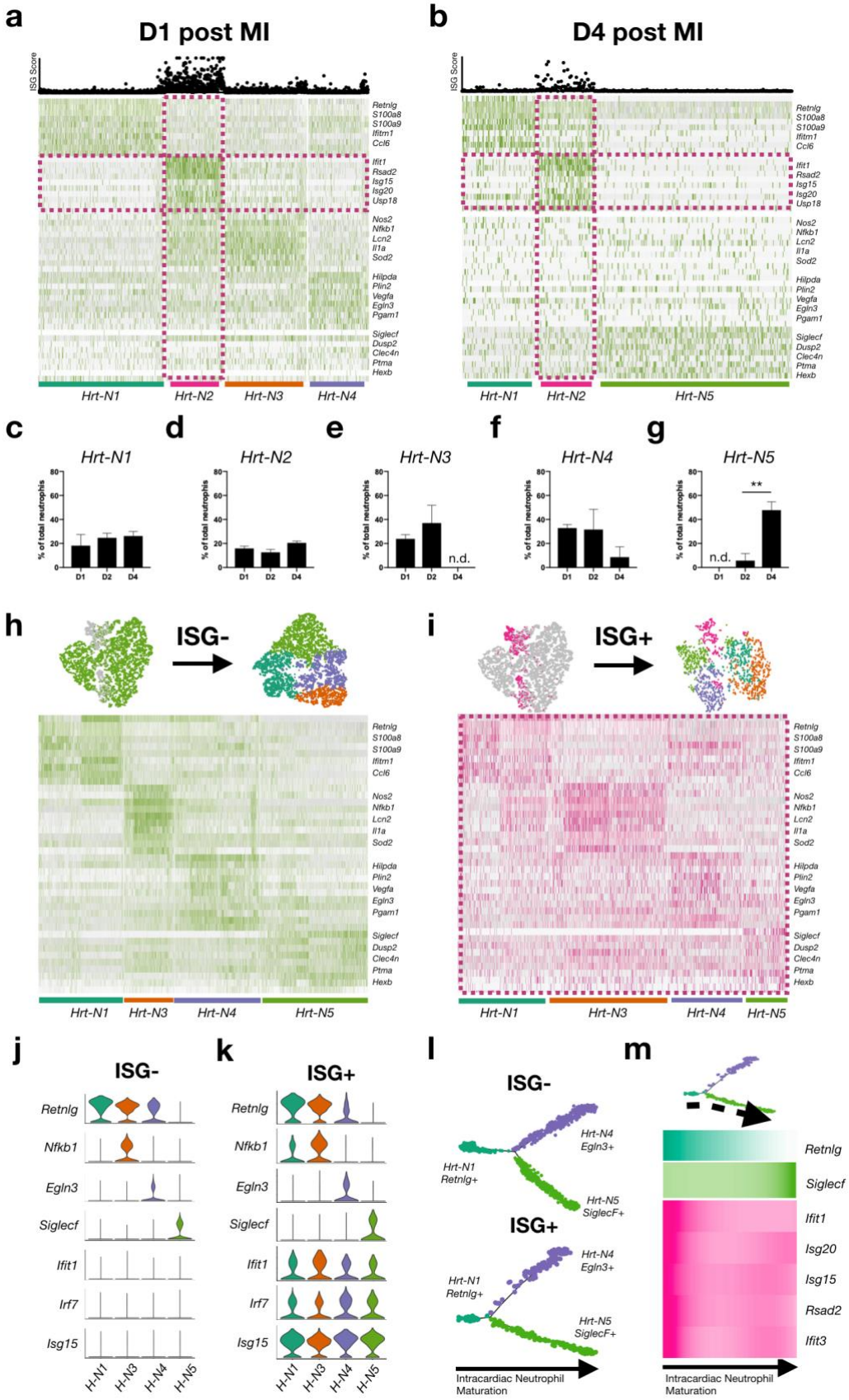
a
D1 post MI
ISG Score
Retnlg
S100a8
S100a9
Ifitm1
Ccl6
Ifit1
Rsad2
Isg15
Isg20
Usp18
Nos2
Nfkb1
Lcn2
Il1a
Sod2
Hilpda
Plin2
Vegfa
Egln3
Pgam1
Siglecf
Dusp2
Clec4n
Ptma
Hexb
Hrt-N1
Hrt-N2
Hrt-N3
Hrt-N4
b
D4 post MI
Hrt-N5
c
Hrt-N1
d
Hrt-N2
e
Hrt-N3
f
Hrt-N4
g
Hrt-N5
% of total neutrophils
D1
D2
D4
n.d.
**
h
ISG-
i
ISG+
j
ISG-
k
ISG+
Irf7
H-N1
H-N3
H-N4
H-N5
l
Hrt-N4
Egln3+
Hrt-N1
Retnlg+
Hrt-N5
SiglecF+
Intracardiac Neutrophil
Maturation
m
Ifit3

Figure 2. Intracardiac neutrophils exhibit mirrored ISG+ and ISG- cell subsets after MI. a-b) Representative heatmap and ISG score of intracardiac neutrophils on **a)** days 1 (n = 2,285 cells, 1 mouse) and **b)** day 4 (n = 720 cells, 1 mouse) after MI (ISG-expressing cells and marker genes outlined in pink). **c-g)** Amounts of neutrophils subsets **c)** Hrt-N1 **d)** Hrt-N2 **e)** Hrt-N3 **f)** Hrt-N4 **g)** Hrt-N5 on days 1, 2 and 4 after MI. Comparisons across time are non-significant unless otherwise noted. **h-i)** t-SNE map and heatmap of combined, subsetted and reclustered neutrophils from **h)** ISG- and **i)** ISG+ populations across all days. **j-k)** Violin plots of **j)** ISG- and **k)** ISG+ neutrophils. **l-m)** Pseudotime trajectory analysis of **l)** ISG- and ISG+ neutrophils and **m)** heatmap of neutrophil maturation and ISG expression vs pseudotime from $Retnlg^{HI}Siglecf^{LOW}$ to $Retnlg^{LOW}Siglecf^{HI}$ (induced by dotted arrow). Heatmaps show z-score ranging from -2.5 (white), 0 (grey), and +2.5 (green for **a,b,h** or pink for **i**). Data are shown as mean ± s.e.m. ** *P< 0.01,* unpaired two-sided student t-test.

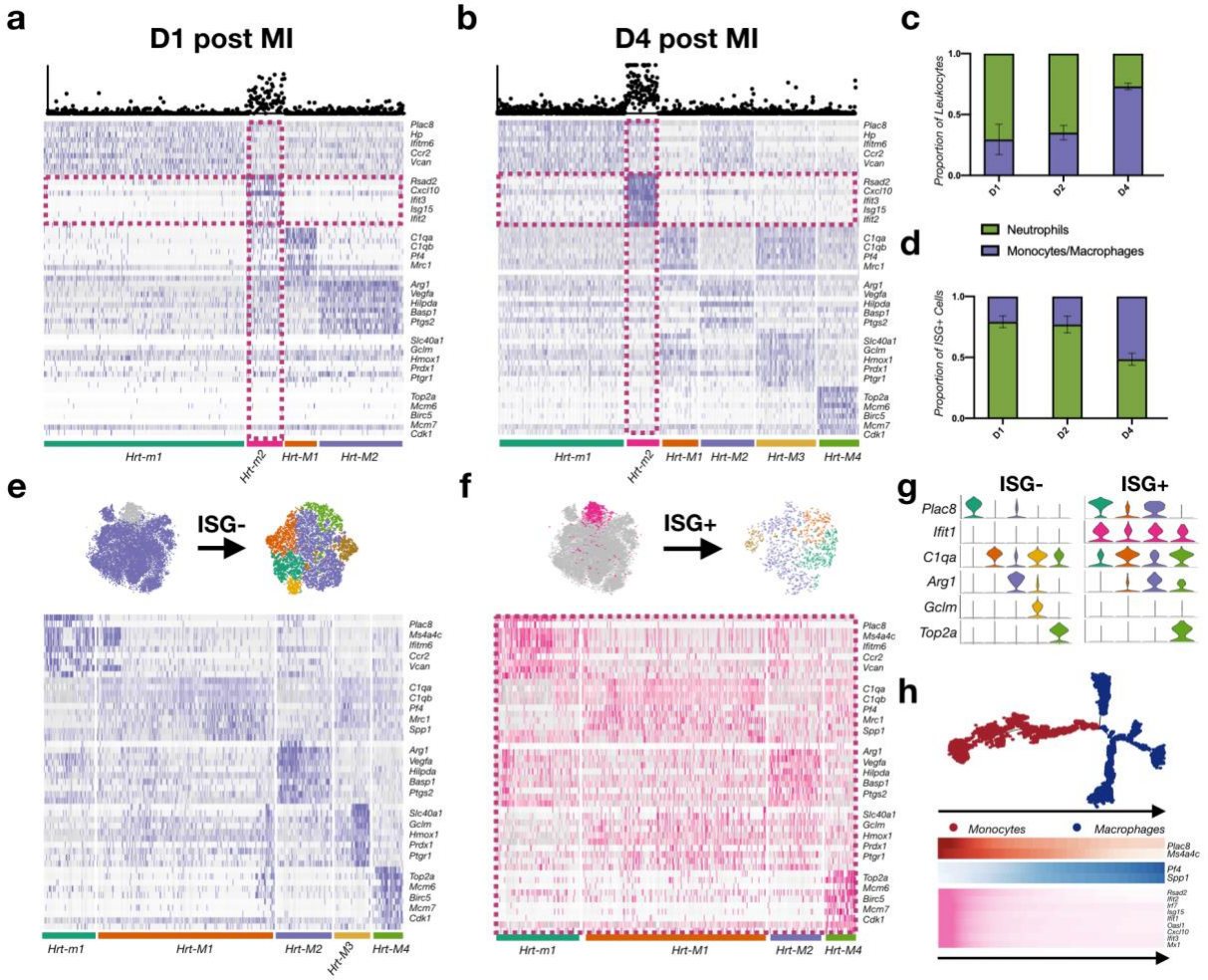

Figure 3. Intracardiac monocytes, and macrophages exhibit mirrored ISG+ and ISG- cell subsets after MI. a-b) Representative heatmap and ISG score of intracardiac monocytes and macrophages on **a)** days 1 (n = 987 cells, 2 mice) and **b)** day 4 (n = 1723 cells, 1 mouse) after MI. **c-d)** Proportion of neutrophils (green) and monocytes/macrophages (blue) of **c)** leukocytes and **d)** ISG positive cells on days 1, 2, and 4 post MI. **e-f)** t-SNE map and heatmap of combined, subsetted and reclustered monocytes/macrophages from **e)** ISG- and **f)** ISG+ populations across all days. **g)** Violin plot of marker genes for reclustered ISG+ and ISG- subsets. **h)** Pseudotime trajectory analysis of intracardiac monocytes/macrophages on day 4 after MI and heatmap of monocyte marker genes (red), macrophage marker genes (blue), and ISGs (pink) vs. pseudotime, z-score ranging from -2.5 (white) to 2.5 (indicated color). Heatmaps **(a,b,e,f)** show gene z-score ranging from -2.5 (white), 0 (grey), and +2.5 (blue for **a,b,e** or pink for **f**). Data are shown as mean ± s.e.m.

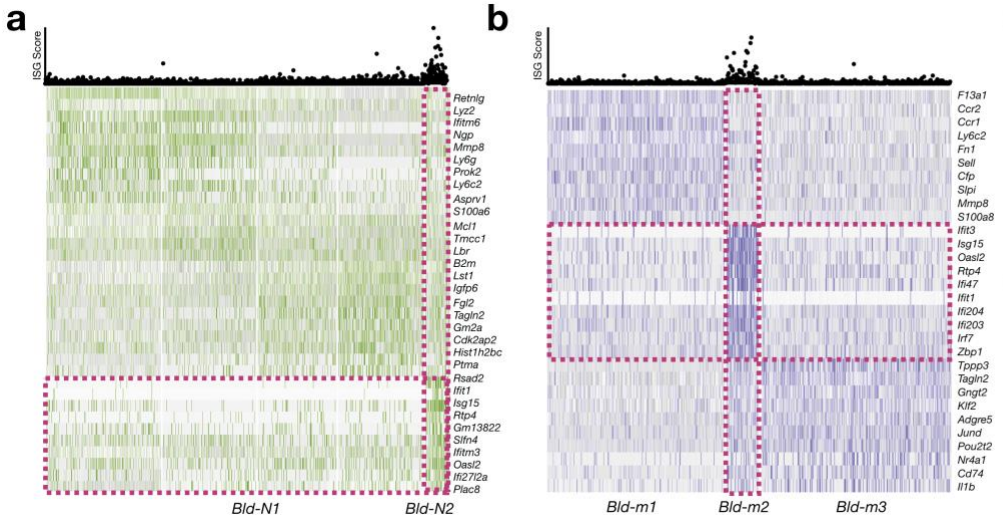

Figure 4. Blood neutrophils and monocytes exist as mirrored ISG+ and ISG- subsets after MI. a-b) Representative heatmap and ISG score of blood **a)** neutrophils (n 2,658 cells, 1 mouse) and **b)** monocytes (n = 974, 1 mouse) on day 1 and day 4 after MI, respectively. **c-d)** ISG score distribution and comparison across **c)** neutrophil subsets and **b)** monocyte subsets in blood. Heatmaps **(a,b)** show gene z-scores ranging from -2.5 (white), 0 (grey), and +2.5 (green for **a** or blue for **e**). Data are shown as mean + s.e.m. ****P<0.0001, two-sided Mann-Whitney test.

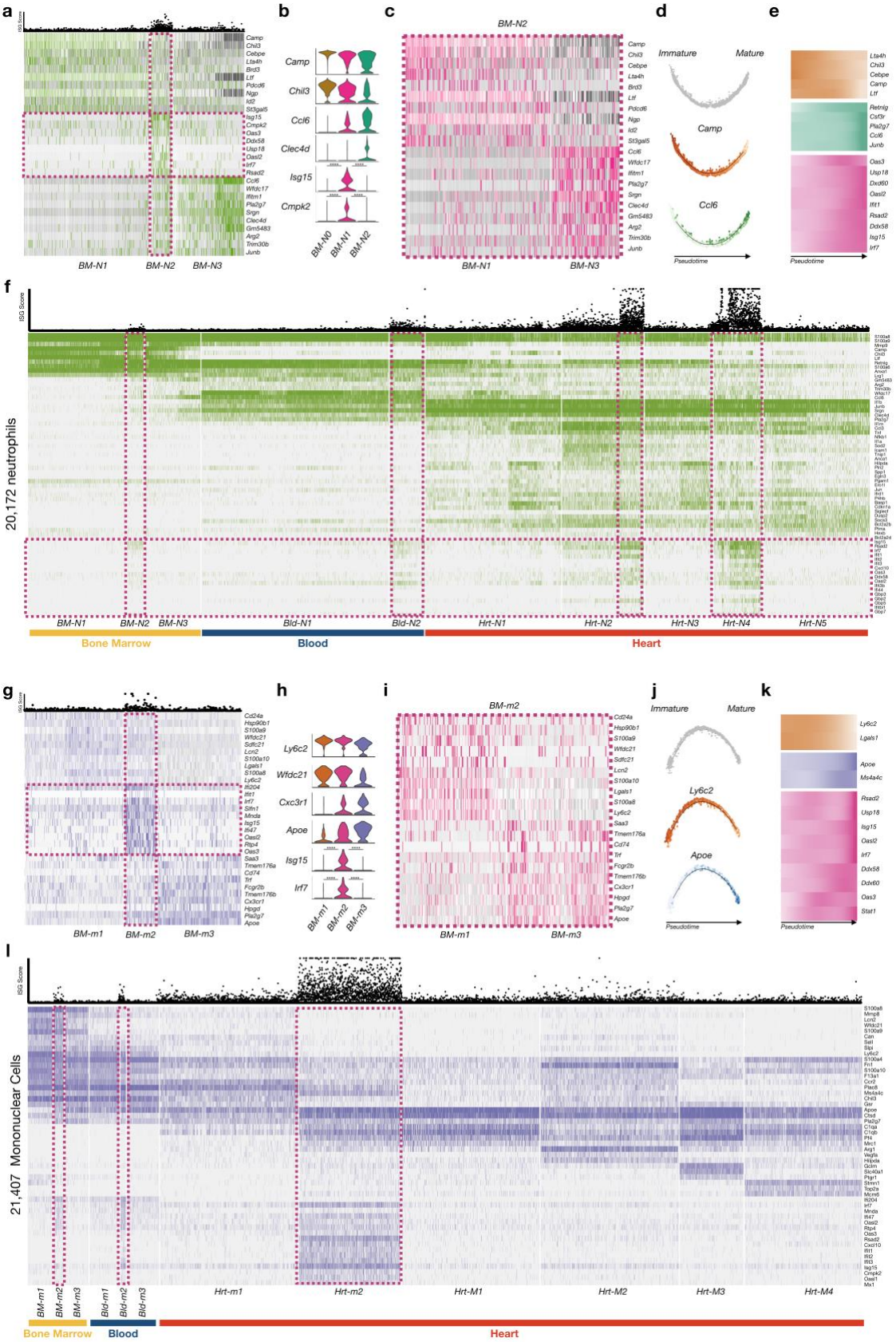
a
b
c
d
e
f
g
h
i
j
k
l
ISG Score
BM-N1
BM-N2
BM-N3
BM-N0
Camp
Chil3
Ccl6
Clec4d
Isg15
Cmpk2
Immature
Mature
Pseudotime
Bld-N1
Bld-N2
Hrt-N1
Hrt-N2
Hrt-N3
Hrt-N4
Hrt-N5
Bone Marrow
Blood
Heart
20,172 neutrophils
BM-m1
BM-m2
BM-m3
Ly6c2
Wfdc21
Cxc3r1
Apoe
Irf7
Hrt-m1
Hrt-m2
Hrt-M1
Hrt-M2
Hrt-M3
Hrt-M4
21,407 Mononuclear Cells

Figure 5. Bone marrow neutrophils and monocytes exist as mirrored ISG+ and ISG- cell subsets after MI. a) Heatmap and ISG score of bone marrow neutrophils of combined data from days 1, 2 and 3 after MI (n = 4473 cells, 3 mice). **b)** Violin plot shows immature ISG- (brown), and mature ISG+ (pink) and ISG- (green) bone marrow neutrophils on days 1-3 after MI. **c)** Heatmap of isolated and reclustered ISG+ neutrophils reveal immature and mature subsets. **d)** Pseudotime trajectory map of neutrophil maturation with representative marker genes of immature (*Camp,* orange) and mature neutrophils (*Ccl6,* green). **e)** Heatmap of neutrophil immature marker genes (orange), mature marker genes (green) and ISGs (pink) vs pseudotime. **f)** Heatmap and ISG score of bone marrow, blood, and intracardiac neutrophils after MI with select genes showing maturation and specialization. **g)** Heatmap and ISG score of bone marrow monocytes of combined data from days 1, 2 and 3 after MI (n = 1382 cells, 3 mice). **h)** Violin plot shows immature ISG- (orange), and mature ISG+ (pink) and ISG- (blue) bone marrow monocytes on days 1-3 after MI. **i)** Heatmap of isolated and reclustered ISG+ monocytes reveals immature and mature subsets. **j)** Pseudotime trajectory map of monocyte maturation with representative marker genes of immature (*Ly6c2,* orange) and mature monocytes (*Apoe,* blue). **k)** Heatmap of neutrophil immature marker genes (orange), mature marker genes (blue) and ISGs (pink) vs pseudotime. **l)** Heatmap and ISG score of bone marrow, blood, and intracardiac monocytes and macrophages from all days combined after MI with select genes showing maturation and specialization. Heatmaps **(a,c,f,g,i,l)** show gene z-score ranging from -2.5 (white), 0 (grey), and +2.5 (green for **a, f;** blue for **g,l**; pink for **c,i**). ****P<0.0001, Mann-Whitney test.

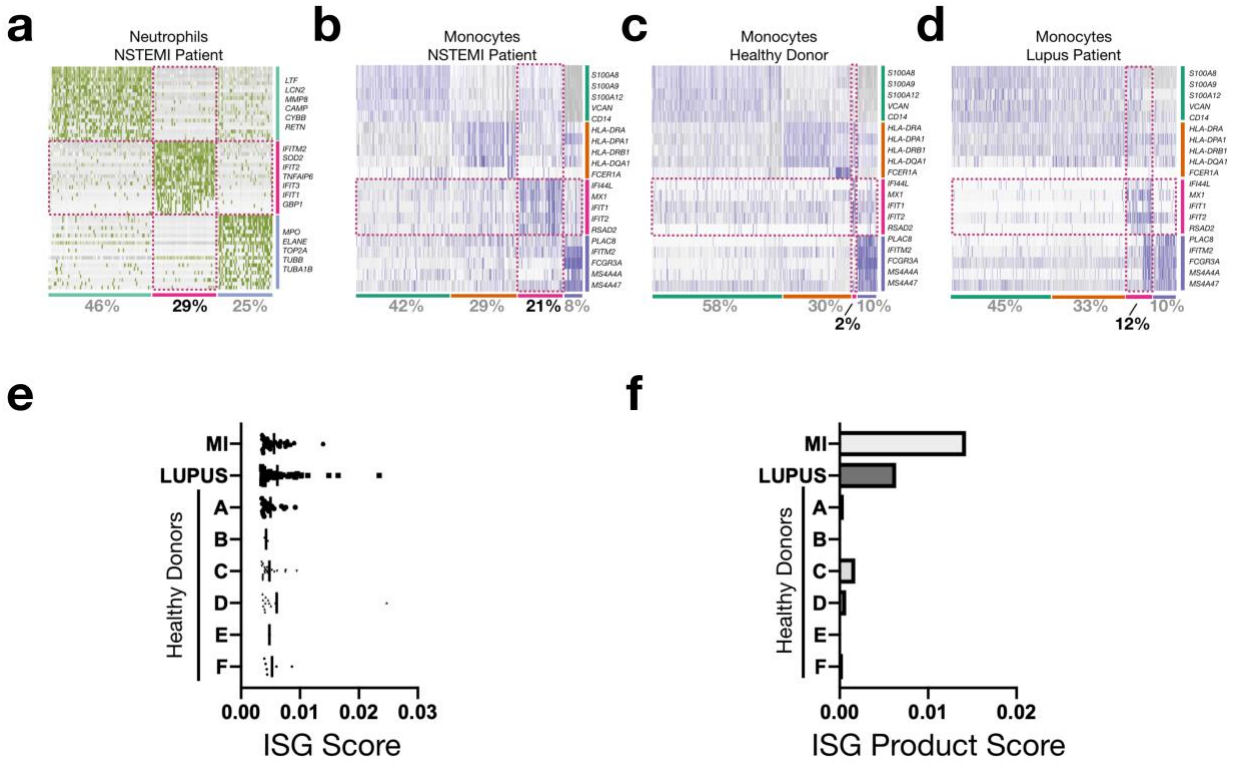

Figure 6. Human blood neutrophils and monocytes after acute myocardial infarction. a-b) Heatmap of human blood **a)** neutrophils after MI (n = 188 cells, 1 patient) and **b)** monocytes after MI (n = 481 cells, 1 patient), **c)** monocytes from a representative healthy donor (n = 2,219 cells, 1 patient), and **d)** monocytes from lupus patients (n= 3,395 cells, 8 patients) highlighting ISG+ cell clusters and marker genes (pink dotted line). **e)** ISG score of human peripheral blood monocyte RNA-Seq transcriptomes from acute MI patient (n = 2,335 cells, 1 patient), lupus patients (n = 3,395 cells, 8 patients), and healthy donors (n = 10,392 cells, 6 patients). **f)** ISG product score of monocytes from acute MI patient (n = 2,335 cells, 1 patient), lupus patients (n = 3,395 cells, 8 patients), and healthy donors (10,392 cells, 6 patients) calculated from single cell RNA-Seq data of human peripheral blood based upon a 99th percentile ISG score threshold as detailed in methods. Heatmaps **(a-d)** show gene z-score ranging from -2.5 (white), 0 (grey), and +2.5 (green for **a;** blue for **b-d**). * *P < 0.05,* *** *P < .001,* ****P<0.0001, Mann-Whitney test.

REFERENCES

1 Ito, K. & Frenette, P. S. HSC Contribution in Making Steady-State Blood. *Immunity* **45**, 464-466, doi:10.1016/j.immuni.2016.09.002 (2016).

2 Mendez-Ferrer, S., Chow, A., Merad, M. & Frenette, P. S. Circadian rhythms influence hematopoietic stem cells. *Curr Opin Hematol* **16**, 235-242, doi:10.1097/MOH.0b013e32832bd0f5 (2009).

3 Mendez-Ferrer, S. & Frenette, P. S. Hematopoietic stem cell trafficking: regulated adhesion and attraction to bone marrow microenvironment. *Ann N Y Acad Sci* **1116**, 392-413, doi:10.1196/annals.1402.086 (2007).

4 Hanna, R. N. *et al.* The transcription factor NR4A1 (Nur77) controls bone marrow differentiation and the survival of Ly6C- monocytes. *Nat Immunol* **12**, 778-785, doi:10.1038/ni.2063 (2011).

5 Mildner, A. *et al.* Genomic Characterization of Murine Monocytes Reveals C/EBPbeta Transcription Factor Dependence of Ly6C(-) Cells. *Immunity* **46**, 849-862 e847, doi:10.1016/j.immuni.2017.04.018 (2017).

6 Boettcher, S. & Manz, M. G. Regulation of Inflammation- and Infection-Driven Hematopoiesis. *Trends Immunol* **38**, 345-357, doi:10.1016/j.it.2017.01.004 (2017).

7 Dutta, P. *et al.* Myocardial Infarction Activates CCR2(+) Hematopoietic Stem and Progenitor Cells. *Cell Stem Cell* **16**, 477-487, doi:10.1016/j.stem.2015.04.008 (2015).

8 Herault, A. *et al.* Myeloid progenitor cluster formation drives emergency and leukaemic myelopoiesis. *Nature* **544**, 53-58, doi:10.1038/nature21693 (2017).

9 Manz, M. G. & Boettcher, S. Emergency granulopoiesis. *Nat Rev Immunol* **14**, 302-314, doi:10.1038/nri3660 (2014).

10 Kaczmarek, A., Vandenabeele, P. & Krysko, D. V. Necroptosis: the release of damage-associated molecular patterns and its physiological relevance. *Immunity* **38**, 209-223, doi:10.1016/j.immuni.2013.02.003 (2013).

11 Dick, S. A. *et al.* Self-renewing resident cardiac macrophages limit adverse remodeling following myocardial infarction. *Nat Immunol* **20**, 29-39, doi:10.1038/s41590-018-0272-2 (2019).

12 Epelman, S., Lavine, K. J. & Randolph, G. J. Origin and functions of tissue macrophages. *Immunity* **41**, 21-35, doi:10.1016/j.immuni.2014.06.013 (2014).

13 Epelman, S., Liu, P. P. & Mann, D. L. Role of innate and adaptive immune mechanisms in cardiac injury and repair. *Nat Rev Immunol* **15**, 117-129, doi:10.1038/nri3800 (2015).

14 King, K. R. *et al.* IRF3 and type I interferons fuel a fatal response to myocardial infarction. *Nat Med* **23**, 1481-1487, doi:10.1038/nm.4428 (2017).

15 Nahrendorf, M. *et al.* The healing myocardium sequentially mobilizes two monocyte subsets with divergent and complementary functions. *J Exp Med* **204**, 3037-3047, doi:10.1084/jem.20070885 (2007).

16 Ng, L. G., Ostuni, R. & Hidalgo, A. Heterogeneity of neutrophils. *Nat Rev Immunol* **19**, 255-265, doi:10.1038/s41577-019-0141-8 (2019).

17 Silvestre-Roig, C., Hidalgo, A. & Soehnlein, O. Neutrophil heterogeneity: implications for homeostasis and pathogenesis. *Blood* **127**, 2173-2181, doi:10.1182/blood-2016-01-688887 (2016).

18 Walmsley, S. R. *et al.* Prolyl hydroxylase 3 (PHD3) is essential for hypoxic regulation of neutrophilic inflammation in humans and mice. *J Clin Invest* **121**, 1053-1063, doi:10.1172/JCI43273 (2011).

19 Engblom, C. *et al.* Osteoblasts remotely supply lung tumors with cancer-promoting SiglecF(high) neutrophils. *Science* **358**, doi:10.1126/science.aal5081 (2017).

20 Qiu, X. *et al.* Reversed graph embedding resolves complex single-cell trajectories. *Nat Methods* **14**, 979-982, doi:10.1038/nmeth.4402 (2017).

21 Shalek, A. K. *et al.* Single-cell transcriptomics reveals bimodality in expression and splicing in immune cells. *Nature* **498**, 236-240, doi:10.1038/nature12172 (2013).

22 Shalek, A. K. *et al.* Single-cell RNA-seq reveals dynamic paracrine control of cellular variation. *Nature* **510**, 363-369, doi:10.1038/nature13437 (2014).

23 Muller, U. *et al.* Functional role of type I and type II interferons in antiviral defense. *Science* **264**, 1918-1921, doi:10.1126/science.8009221 (1994).

24 Essers, M. A. *et al.* IFNalpha activates dormant haematopoietic stem cells in vivo. *Nature* **458**, 904-908, doi:10.1038/nature07815 (2009).

25 Sager, H. B. *et al.* Targeting Interleukin-1beta Reduces Leukocyte Production After Acute Myocardial Infarction. *Circulation* **132**, 1880-1890, doi:10.1161/CIRCULATIONAHA.115.016160 (2015).

26 Dutta, P. *et al.* Myocardial infarction accelerates atherosclerosis. *Nature* **487**, 325-329, doi:10.1038/nature11260 (2012).

27 Cao, D. J. *et al.* Cytosolic DNA Sensing Promotes Macrophage Transformation and Governs Myocardial Ischemic Injury. *Circulation* **137**, 2613-2634, doi:10.1161/CIRCULATIONAHA.117.031046 (2018).

28 Ablasser, A. *et al.* Cell intrinsic immunity spreads to bystander cells via the intercellular transfer of cGAMP. *Nature* **503**, 530-534, doi:10.1038/nature12640 (2013).

29 Patel, S. J., King, K. R., Casali, M. & Yarmush, M. L. DNA-triggered innate immune responses are propagated by gap junction communication. *Proc Natl Acad Sci U S A* **106**, 12867-12872, doi:10.1073/pnas.0809292106 (2009).

30 Pinho, S. & Frenette, P. S. Haematopoietic stem cell activity and interactions with the niche. *Nat Rev Mol Cell Biol* **20**, 303-320, doi:10.1038/s41580-019-0103-9 (2019).

31 Tikhonova, A. N. *et al.* The bone marrow microenvironment at single-cell resolution. *Nature* **569**, 222-228, doi:10.1038/s41586-019-1104-8 (2019).

32 Li, T. & Chen, Z. J. The cGAS-cGAMP-STING pathway connects DNA damage to inflammation, senescence, and cancer. *J Exp Med* **215**, 1287-1299, doi:10.1084/jem.20180139 (2018).

33 Harding, S. M. *et al.* Mitotic progression following DNA damage enables pattern recognition within micronuclei. *Nature* **548**, 466-470, doi:10.1038/nature23470 (2017).

34 Mackenzie, K. J. *et al.* cGAS surveillance of micronuclei links genome instability to innate immunity. *Nature* **548**, 461-465, doi:10.1038/nature23449 (2017).

35 Denais, C. M. *et al.* Nuclear envelope rupture and repair during cancer cell migration. *Science* **352**, 353-358, doi:10.1126/science.aad7297 (2016).

36 Raab, M. *et al.* ESCRT III repairs nuclear envelope ruptures during cell migration to limit DNA damage and cell death. *Science* **352**, 359-362, doi:10.1126/science.aad7611 (2016).

37 Ridker, P. M. High-sensitivity C-reactive protein, inflammation, and cardiovascular risk: from concept to clinical practice to clinical benefit. *Am Heart J* **148**, S19-26, doi:10.1016/j.ahj.2004.04.028 (2004).

38 Ridker, P. M., Hennekens, C. H., Buring, J. E. & Rifai, N. C-reactive protein and other markers of inflammation in the prediction of cardiovascular disease in women. *N Engl J Med* **342**, 836-843, doi:10.1056/NEJM200003233421202 (2000).

39 Ridker, P. M. *et al.* Antiinflammatory Therapy with Canakinumab for Atherosclerotic Disease. *N Engl J Med* **377**, 1119-1131, doi:10.1056/NEJMoa1707914 (2017).

40 Furie, R. *et al.* Anifrolumab, an Anti-Interferon-alpha Receptor Monoclonal Antibody, in Moderate-to-Severe Systemic Lupus Erythematosus. *Arthritis Rheumatol* **69**, 376-386, doi:10.1002/art.39962 (2017).

41 Nestorowa, S. *et al.* A single-cell resolution map of mouse hematopoietic stem and progenitor cell differentiation. *Blood* **128**, e20-31, doi:10.1182/blood-2016-05-716480 (2016).

42 Klein, A. M. *et al.* Droplet barcoding for single-cell transcriptomics applied to embryonic stem cells. *Cell* **161**, 1187-1201, doi:10.1016/j.cell.2015.04.044 (2015).

43 Zilionis, R. *et al.* Single-cell barcoding and sequencing using droplet microfluidics. *Nat Protoc* **12**, 44-73, doi:10.1038/nprot.2016.154 (2017).